NASA Contractor Report 194971

ICASE Report No. 94-73

ICASE

SPECTRAL SOLUTION OF THE VISCOUS BLUNT BODY PROBLEM. II: MULTIDOMAIN APPROXIMATION

David A. Kopriva

Contract NAS1-19480
August 1994

Institute for Computer Applications in Science and Engineering
NASA Langley Research Center
Hampton, VA 23681-0001

Operated by Universities Space Research Association

SPECTRAL SOLUTION OF THE VISCOUS BLUNT BODY PROBLEM. II: MULTIDOMAIN APPROXIMATION

David A. Kopriva[1]
The Florida State University
Tallahassee, FL 32306

ABSTRACT

We present steady solutions of high speed viscous flows over blunt bodies using a multidomain Chebyshev spectral collocation method. The region within the shock layer is divided into subdomains so that internal layers can be well-resolved. In the interiors of the subdomains, the solution is approximated by Chebyshev collocation. At interfaces between subdomains, the advective terms are upwinded and the viscous terms are treated by a penalty method. The method is applied to five flows the Mach number range 5-25 and Reynolds number range 2,000 - 83,000, based on nose radius. Results are compared to experimental data and to a finite difference result.

[1]Research was supported by the National Aeronautics and Space Administration under NASA Contract No. NAS1-19480 while the author was in residence at the Institute for Computer Applications in Science and Engineering (ICASE), NASA Langley Research Center, Hampton, VA 23681-0001. Research was also supported under NASA Contract No. NAG1-862 and by the U.S. Department of Energy through Contract No. DE-FC05-85ER250000.

Introduction

Spectral methods are now applied to a wide variety of fluid dynamics problems[1]. They are characterized by global, high order orthogonal polynomial approximations. For smooth enough solutions they give exponential order convergence. The high order approximation of the advective terms has low dissipation errors, which is important in viscous flow calculations.

Compared to finite difference methods, fewer grid points are needed by spectral methods to obtain highly accurate solutions. As an example, Pruett and Streett[2] compared the results of a Chebyshev method for the solution of the compressible boundary layer equations to that of a second order finite difference method. To compute the wall temperature for an adiabatic wall, they found that 77 points were required for the spectral method to obtain the same five digit accuracy for which the finite difference method required 400.

On the negative side, the use of global polynomial approximations makes it difficult to solve problems with multiple length scales. These scales might be associated with the size of an aerodynamic body, the distance between shock waves, the size of entropy and vorticity layers, and the size of viscous boundary layers. A standard spectral collocation method would require a complex mapping and a large number of grid points to solve such problems. Refinement of the grid to resolve local features would have to be handled by the mappings. The resulting problem would be numerically very stiff. Very small time-steps and large numbers of iterations would be required to converge to steady-state.

To ameliorate the difficulties of standard spectral methods, multidomain spectral methods have been developed to solve incompressible viscous (see Ref. 1 for a discussion) and, now, compressible[3-7] flows. Multidomain methods still give the exponential error convergence characteristic of the spectral methods, but also allow for local refinement of the grid.

In this paper, we apply to the solution of the steady blunt body problem a new multidomain Chebyshev collocation method developed for the solution of the compressible Navier-Stokes equations[8]. The important feature of the method is the treatment of the interfaces between subdomains. At a subdomain interface, the advective terms in the equations are treated by an upwind characteristic correction procedure developed for the inviscid Euler gas-dynamics equations.[3] The viscous terms are approximated by a weighted average of the

terms on either side plus a penalty term proportional to the jump in the viscous fluxes. The result is a method with communication limited to the passing of boundary data only.

The method is applied to five examples. The first four examples are of sphere, cylinder and blunt cone geometries at Mach number 5.73 and 10.6. For these solutions, the surface pressure or the heat transfer are compared to experiments. The final problem is the solution of a Mach 25 flow over a hyperbolic cone. This problem was solved earlier by a single domain spectral method.[9] The results are compared to a finite difference Thin Layer Navier-Stokes calculation and to the single domain solution.

The Blunt Body Problem

In this paper we solve for viscous supersonic flow about a blunt nose cone at zero angle of attack. Fig. 1 shows a diagram of the situation. Spectral approximations of this problem using single domains have been performed by Kopriva[9] and Yasuhara, Nakamura and Wang[10]. Because of the symmetry along the centerline of the body, we need to solve only the upper half of the full flow problem. For high Mach and Reynolds numbers, the bow shock can be viewed as a discontinuity.[7] By fitting the shock as a boundary to the flow, then, we consider the solution only in the shock-layer.

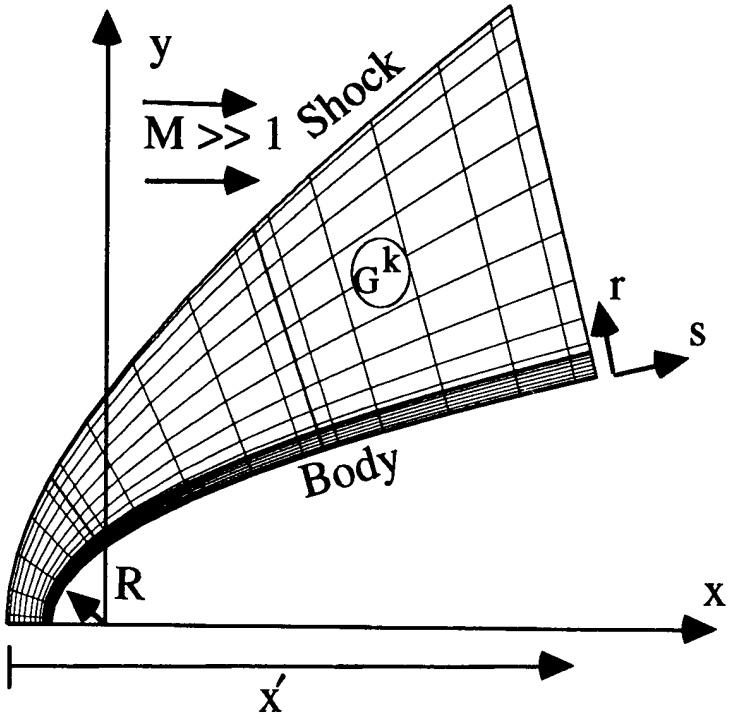

Fig. 1 Diagram of the blunt body geometry. The gridded area represents the computation region subdivided into multiple subdomains

We approximate the compressible Navier-Stokes equations in the non-conservative form

$$\begin{aligned}
&\rho_t + u\rho_x + v\rho_y + \rho u_x + \rho v_y + \frac{\rho v \xi}{y} = 0 \\
&u_t + uu_x + vu_y + \frac{p_x}{\rho} = \frac{\sqrt{\gamma} M_{ref}}{\rho \mathrm{Re}} \tau^x \\
&v_t + uv_x + vv_y + \frac{p_y}{\rho} = \frac{\sqrt{\gamma} M_{ref}}{\rho \mathrm{Re}} \tau^y \\
&p_t + up_x + vp_y + \gamma p\left(u_x + v_y + \frac{v\xi}{y}\right) \\
&\quad = \frac{\gamma\sqrt{\gamma} M_{ref}}{\mathrm{Pr}\,\mathrm{Re}} \nabla \bullet (\kappa \nabla T) + \frac{(\gamma - 1)\sqrt{\gamma} M_{ref}}{\mathrm{Re}} \Phi
\end{aligned} \tag{1}$$

where

$$\begin{aligned}
\tau^x &= \frac{\partial}{\partial x}\left(\mu(4u_x - 2v_y)/3 - \frac{2\mu v}{3y}\right) + \frac{\partial}{\partial y}\left(\mu(v_x + u_y)\right) \\
&\quad + \frac{\xi\mu}{y}(v_x + u_y) \\
\tau^y &= \frac{\partial}{\partial x}\left(\mu(v_x + u_y)\right) + \frac{\partial}{\partial y}\left(\mu(4v_y - 2u_x)/3 - \frac{2\mu v\xi}{3y}\right) \\
&\quad + \frac{2\mu\xi}{y}\left(v_y - \frac{v}{y}\right)
\end{aligned} \tag{2a}$$

and

$$\begin{aligned}
\Phi = &\frac{\mu u_x}{3}\left(4u_x - 2v_y\right) + \mu(u_y + v_x)^2 + \frac{\mu v_y}{3}\left(4v_y - 2u_x\right) + \\
&\frac{4\mu\xi}{3}\left(\left(\frac{v}{y}\right)^2 - \frac{v}{y}(u_x + v_y)\right)
\end{aligned} \tag{2b}$$

The parameter $\xi = 1$ for axisymmetric flow and $\xi = 0$ otherwise.

In these equations, we have scaled the dimensional pressure, density, velocity and temperature (p^*, ρ^*, q^*, T^*) by

$$\begin{aligned}
p &= p^* / p_{ref} \\
\rho &= \rho^* / \rho_{ref} \\
\mathbf{q} &= (u, v) = \mathbf{q}^* / \sqrt{p_{ref} / \rho_{ref}}
\end{aligned} \tag{3a}$$

$$T = T^* / \left(\frac{p_{ref}}{\Re \rho_{ref}} \right)$$

where $\Re$ is the gas constant. We scale the dimensional space and time by

$$\mathbf{x} = \mathbf{x}^* / L \tag{3b}$$
$$t = \sqrt{p_{ref} / \rho_{ref}}\, t^* / L,$$

where L represents the length scale. For the blunt body problems computed here, we choose p_{ref} and ρ_{ref} to be the free stream values and L to be the nose radius.

The temperature is computed by the perfect gas equation of state, which becomes

$$T = p/\rho \tag{4}$$

under the scaling (3). The dimensionless variables in (1) are the standard Reynolds Number (Re), which is scaled to the characteristic length, the Prandtl Number (Pr) and the Mach Number (M).

To compute the viscosity coefficient, we use the Sutherland law

$$\mu = \frac{\mu^*}{\mu_{ref}} = \frac{1 + 198.6 / T_{ref}}{T + 198.6 / T_{ref}} T^{3/2} \tag{5}$$

where T_{ref} is measured in ^{o}R. We assume that the Prandtl number is constant, so the same formula is used to compute the dimensionless heat conductivity, κ.

The Multidomain Spectral Method

The multidomain method that we use is presented in Kopriva[8]. As before, we consider non-overlapping and "conforming" approximations only. By conforming we mean that subdomains intersect only along a side or at a point, and that grid lines must be continuous between subdomains. However, in this paper, the geometry is allowed to change with time (because of the moving shock) and axisymmetric geometry is considered. The moving grid requires the interface conditions to change at each time step.

The domain decomposition for the blunt body problem is performed as described in Kopriva[4,5]. We subdivide the region between the shock and the body into multiple non-overlapping subdomains, G^k, which collectively cover the region between the shock and the body. (See Fig. 1) Each subdomain is bounded by four curves. In the direction normal to the body, r, the bounds are $r^k_{\min}(s,t)$ and $r^k_{\max}(s,t)$. Time dependent subdomain boundary positions are included to allow the shock boundary to move with time. For convenience

only, we require the subdomains to be bounded in the body tangential direction, s, by straight lines normal to the body surface.

Given the boundary curves on a subdomain, a mapping from $(r,s,t) \leftrightarrow (X,Y,T)$ is used:

$$
\begin{aligned}
X^k &= \frac{r - r^k_{\min}(s,t)}{r^k_{\max}(s,t) - r^k_{\min}(s,t)} \\
Y^k &= \frac{s - s^k_{\min}}{s^k_{\max} - s^k_{\min}} \\
\tau &= t
\end{aligned}
\tag{6}
$$

For each subdomain the (6) transformation causes the equations (1) to be rewritten as

$$
\begin{aligned}
\rho_\tau + A_\rho &= 0 \\
u_\tau + A_u &= V_u \\
v_\tau + A_v &= V_v \\
p_\tau + A_p &= V_p
\end{aligned}
\tag{7}
$$

In (7), the advective terms are

$$
\begin{aligned}
A_\rho &= U\rho_X + V\rho_Y + \rho u_X + \rho v_Y + \frac{\rho v \xi}{y} \\
A_u &= Uu_X + Vu_Y + \frac{1}{\rho}\left(X_x p_X + Y_x p_Y\right) \\
A_v &= Uv_X + Vv_Y + \frac{1}{\rho}\left(X_y p_X + Y_y p_Y\right) \\
A_p &= Up_X + Vp_Y + \gamma p\left(X_x u_X + Y_x u_Y + X_y v_X + Y_y v_Y + \frac{v\xi}{y}\right)
\end{aligned}
\tag{8}
$$

where

$$
\begin{aligned}
U &= X_t + uX_x + vX_y \\
V &= uY_x + vY_y
\end{aligned}
$$

For convenience, we have left off the superscripts that denote the subdomain. The viscous terms are

$$
\begin{aligned}
V_u &= \frac{\sqrt{\gamma}M_{ref}}{\rho \mathrm{Re}}\left\{\frac{1}{J}\left(\frac{\partial}{\partial X}\left(\tilde{F}_u\right) + \frac{\partial}{\partial Y}\left(\tilde{G}_u\right)\right) + \frac{\mu\xi}{y}\left(X_x v_X + Y_x v_Y + X_y u_X + Y_y u_Y\right)\right\} \\
V_v &= \frac{\sqrt{\gamma}M_{ref}}{\rho \mathrm{Re}}\left\{\frac{1}{J}\left(\frac{\partial}{\partial X}\left(\tilde{F}_v\right) + \frac{\partial}{\partial Y}\left(\tilde{G}_v\right)\right) + \frac{2\mu\xi}{y}\left(X_y v_X + Y_y v_Y - \frac{v}{y}\right)\right\} \\
V_p &= \frac{\gamma\sqrt{\gamma}M_{ref}}{\mathrm{Pr}\,\mathrm{Re}}\frac{1}{J}\left(\frac{\partial}{\partial X}\left(\tilde{F}_p\right) + \frac{\partial}{\partial Y}\left(\tilde{G}_p\right)\right) + \frac{(\gamma-1)\sqrt{\gamma}M_{ref}}{\mathrm{Re}}\Phi
\end{aligned}
\tag{9}
$$

Here, the Jacobian, J, is

$$J = x_X y_Y - x_Y y_X$$

The viscous fluxes in the mapped coordinate are defined to be

$$\begin{aligned} \tilde{F}_q &= y_Y F_q - x_Y G_q \\ \tilde{G}_q &= -y_X F_q + x_X G_q \end{aligned} \tag{10}$$

for $q = u, v,$ or p, and

$$\begin{aligned} F_u &= \mu\Big(4\big(X_x u_X + Y_x u_Y\big) - 2\big(X_y v_X + Y_y v_Y\big)\Big)/3 - \frac{2\mu v\xi}{3y} \\ G_u = F_v &= \mu\big(X_x v_X + Y_x v_Y + X_y u_X + Y_y u_Y\big) \\ G_v &= \mu\Big(4\big(X_x v_X + Y_x v_Y\big) - 2\big(X_y u_X + Y_y u_Y\big)\Big)/3 - \frac{2\mu v\xi}{3y} \\ F_p &= \kappa\big(X_x T_X + Y_x T_Y\big) \\ G_p &= \kappa\big(X_y T_X + Y_y T_Y\big) \end{aligned} \tag{11}$$

Finally,

$$\begin{aligned} \Phi = &\frac{\mu\big(X_x u_X + Y_x u_Y\big)}{3}\Big(4\big(X_x u_X + Y_x u_Y\big) - 2v_y\Big) \\ &+\mu(X_y u_X + Y_y u_Y + X_x v_X + Y_x v_Y)^2 \\ &+\frac{\mu\big(X_y v_X + Y_y v_Y\big)}{3}\Big(4\big(X_y v_X + Y_y v_Y\big) - 2\big(X_x u_X + Y_x u_Y\big)\Big) \\ &+\frac{4\mu\xi}{3}\left(\left(\frac{v}{y}\right)^2 - \frac{v}{y}(X_x u_X + Y_x u_Y + X_y v_X + Y_y v_Y)\right) \end{aligned} \tag{12}$$

We do not multiply through by the Jacobian of the transformation to create new dependent variables, since J can be discontinuous across interfaces between subdomains.

On each subdomain, G^k, we place a grid of points

$$\big(X_i^k, Y_j^k\big) = \left(\frac{1}{2}\left(1 - \cos\left(\frac{i\pi}{N^k}\right)\right), \frac{1}{2}\left(1 - \cos\left(\frac{j\pi}{M^k}\right)\right)\right) \quad \begin{matrix} i = 0,1,2,\ldots,N^k \\ j = 0,1,2,\ldots,M^k \end{matrix} \tag{13}$$

and assign gridpoint values of the solution unknowns, e.g. $p^k_{i,j}$, etc. Derivatives of a solution variable, q (= u,v, or p), are then approximated from the grid point values, $q_{i,j}$, by

$$\left(q_X^k\right)_{i,j} \approx \sum_{l=0}^{N^k} d_{i,l}^{(X)} q_{l,j}^k$$
$$\left(q_Y^k\right)_{i,j} \approx \sum_{l=0}^{M^k} d_{j,l}^{(Y)} q_{i,l}^k \qquad (14)$$

where $d_{i,j}$ is the Chebyshev derivative matrix as written in Ref. 1, pg. 69. We use matrix multiplication rather than FFT's to compute the derivative approximation. FFT's are more efficient for large numbers of points. However, the number of points used here is usually chosen to be fewer than 32, which is around the break-even number of points where the FFT's become faster.

The derivative approximations (14) are substituted into eqns. (8) - (12) to give a system of ordinary differential equations, which we denote as

$$\frac{\partial \rho_{i,j}^k}{\partial t} = -\left(A_\rho\right)_{i,j}^k \qquad (15a)$$

and, for q = each of p, u, or v,

$$\frac{dq_{i,j}^k}{dt} = -\left(A_q\right)_{i,j}^k + \left(V_q\right)_{i,j}^k \qquad (15b)$$

These equations are integrated in time with a second order Runge-Kutta rule.

At interfaces between the subdomains, conditions are applied to allow waves to propagate through them, while weakly enforcing continuity of the viscous flux. To describe the interface method, we consider two subdomains as shown in Fig. 2, one on the left (L) and the other on the right (R) of the interface.

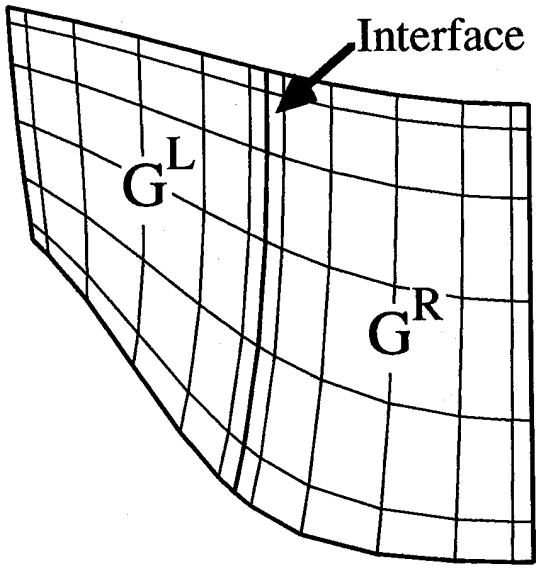

Fig. 2. Diagram of a two subdomain decomposition

At each interface point, we replace the spatial derivatives in (7) by their discrete Chebyshev approximations, (14). Two equations for each grid point on the interface are generated, depending on whether derivatives are computed from the left or from the right. For the density, the equation is purely advective, and we write

$$\frac{\partial \rho^L_{N^L,j}}{\partial t} = -\left(A_\rho\right)^L_{N^L,j}$$
$$\frac{\partial \rho^R_{0,j}}{\partial t} = -\left(A_\rho\right)^R_{0,j} \tag{16a}$$

For q = each of p, u, v, the equations on either side of the interface are written so that the viscosity is approximated by a weighted average of the viscous terms computed on either side of the interface. The continuity required of the viscous flux is enforced weakly by a penalty proportional to the jump in the flux:

$$\frac{dq^L_{N^L,j}}{dt} = -\left(A_q\right)^L_{N^L,j} + \alpha_j\left(V_q\right)^L_{N^L,j} + \beta_j\left(V_q\right)^R_{0,j} + \delta_j\left(\tilde{F}^{\,R}_{q0,j} - \tilde{F}^{\,L}_{qN^L,j}\right)$$
$$\frac{dq^R_{0,j}}{dt} = -\left(A_q\right)^R_{0,j} + \alpha_j\left(V_q\right)^L_{N^L,j} + \beta_j\left(V_q\right)^R_{0,j} + \delta_j\left(\tilde{F}^{\,R}_{q0,j} - \tilde{F}^{\,L}_{qN^L,j}\right) \tag{16b}$$

The weights, α, β, δ depend on the relative sizes of the subdomains, and on the numbers of points in the subdomains:

$$\alpha_j = \frac{J^L_{N^L,j} w^L_{N^L}}{J^L_{N^L,j} w^L_{N^L} + J^R_{0,j} w^R_0},$$
$$\beta_j = \frac{J^R_{0,j} w^R_0}{J^L_{N^L,j} w^L_{N^L} + J^R_{0,j} w^R_0}, \tag{17}$$
$$\delta_j = \frac{1}{J^L_{N^L,j} w^L_{N^L} + J^R_{0,j} w^R_0}$$

The quantities, $w^R_0 = \dfrac{1}{2\left(\left(N^R\right)^2 - 1\right)}$, $w^L_{N^L} = \dfrac{1}{2\left(\left(N^L\right)^2 - 1\right)}$, are the Clenshaw-Curtis quadrature weights defined on the interval [0,1]. Thus, the coefficient of the penalty term grows as $O(N^2)$, and in the limit as $N \to \infty$, (16b) enforces continuity of the flux. To update the solutions, the equations (16) are integrated with a second order Runge-Kutta rule.

An approximation similar to (16) can be written for corner points found at the intersection of four subdomains[8]. At such points, the weighted average is taken over the four values of the diffusion terms, and penalties are applied for the jumps in the diffusive fluxes across each face.

The results of the integration in time are preliminary values of the solutions, $\tilde{\rho}$, $\tilde{p}$, $\tilde{u}$, $\tilde{v}$ on either side of the interface. The preliminary values have used one sided, but not upwind, approximations for the advective terms at the interface points. Thus, these solutions must be corrected to account for wave propagation across the interface. From $\tilde{u},\tilde{v}$, preliminary values of the normal and tangential velocities, $\tilde{w}_1$ and $\tilde{w}_2$, are formed. The preliminary values are then corrected to have the proper advective domain of dependence in the manner described in Ref. 3. For instance, if the flow is subsonic and from left to right across the interface, the choice of four bicharacteristics of the hyperbolic portion of the equations leads to the corrected interface values

$$
\begin{aligned}
p^L_{N^L,j} &= p^R_{0,j} = \frac{1}{2}\left(\tilde{p}^L_{N^L,j} + \tilde{p}^R_{0,j}\right) + \rho^n a^n \left(\left(\tilde{w}_1\right)^L_{N^L,j} - \left(\tilde{w}_1\right)^R_{0,j}\right) \\
\left(w_1\right)^L_{N^L,j} &= \left(w_1\right)^R_{0,j} = \frac{1}{2}\left(\left(\tilde{w}_1\right)^L_{N^L,j} + \left(\tilde{w}_1\right)^R_{0,j}\right) + \frac{1}{\rho^n a^n}\left(\tilde{p}^L_{N^L,j} - \tilde{p}^R_{0,j}\right) \\
\left(w_2\right)^L_{N^L,j} &= \left(w_2\right)^R_{0,j} = \left(w_2\right)^L_{N^L,j} \\
\rho^L_{N^L,j} &= \rho^R_{0,j} = \tilde{\rho}^L_{N^L,j} + \frac{1}{\left(a^n\right)^2}\left(p^L_{N^L,j} - \tilde{p}^L_{N^L,j}\right)
\end{aligned}
\tag{18}
$$

The superscript n refers to the linearization to the previous time level. The velocities u and v can then be computed from the corrected normal and tangential velocities, w_1 and w_2.

The boundary conditions and their approximations are described in detail in Ref. 9. We will only review the basic ideas here. To compute the wall pressure, we use a compatibility equation that relates the pressure and the normal velocity along the inviscid characteristic direction. Thus, the pressure is required to satisfy a combination of both the energy and momentum equations at the body surface. If the surface is adiabatic, this equation uses the normal temperature gradient set equal to zero when the second derivative is computed. The density is computed from the pressure and the temperature either from the equation of state, for an isothermal surface, or, for an adiabatic surface, by a spectral extrapolation that enforces the zero normal temperature gradient.

The shock boundary is treated as a discontinuity by shock fitting since at high Mach and Reynolds numbers, the shock can be considered a sharp discontinuity. The shock-fitting procedure is described in detail in Ref. 4 for the inviscid case. The sharp shock assumption implies that the viscous terms are negligible near the shock, so we ignore them in the calculation of the downstream pressure.

At the outflow boundary, we impose the viscous conditions by setting the normal viscous fluxes to be zero when the second derivatives are computed. Since the streamwise flux is small in high Reynolds number flow, this has little effect on the solution. In the subsonic portion of the boundary layer, we also specify the pressure to be a fixed value, and typically use the inviscid pressure. That pressure can be obtained from a Newtonian flow assumption, which is reasonably accurate for hypersonic flows. It can also be obtained from the solution of the inviscid equations, which we use to start the viscous computation.

Unlike the solutions presented in Ref. 10, no artificial viscosity or spectral filtering are used with this approximation. Filtering of the solution either directly or by the addition of artificial viscous terms is undesirable for three reasons. First, the overall accuracy of the approximation is decreased, since the number of accurate frequencies is reduced. Second, high frequency information is altered. Finally artificial viscous effects can be introduced in the solution. In the absence of shocks or other discontinuities in the computed region, which we avoid here by shock fitting, the need for explicit filtering of smooth solutions often indicates the use of poor boundary procedures that introduce high frequency errors into the solution. These errors destroy both the solution accuracy and, in steady-state problems, the convergence rate.

Solutions

Five problems are solved using the method described above. A summary of the flow parameters is shown below in Table I. The problems include both two-dimensional and axisymmetric flows at a range of Reynolds and Mach Numbers. The solutions for problems I-IV are compared to experimental data. The last problem compares the computed results with a finite difference solution[12].

Table I. Parameters for the Flow Test Cases.

Case	Geometry	M_∞	Re	T_∞	T_W/T_∞	Purpose
I	Sphere	10.6	8.33×10^4	85.21R	Adiab.	Compute C_p
II	Cylinder	5.73	2050	71.37R	71.37	Heat Transfer
III	15° Sphere/Cone	10.6	8.33×10^4	85.21R	Adiab.	C_p
IV	15° Sphere/Cone	10.6	1.65×10^5	85.21 R	6.22	Heat Transfer
V	5° Hyperboloid	25	13,034	486 R	25	Compare with Thin Layer Solution

Case I.

The first problem that we solve is the M = 10.6 flow over a sphere at Reynolds number 83,000 based on nose radius, using a grid with eight subdomains. Fig. 3 shows the computed contours of the pressure, Mach number and temperature along with the grid used. The narrow strip of subdomains along the surface of the sphere was chosen to better resolve the boundary layer. A coarse grid is all that is needed to resolve the essentially inviscid flow outside of the boundary layer. Convergence behavior of the maximum residual over all flow variables, plotted in Fig. 4, shows that steady-state is obtained in double precision (64 bit) arithmetic.

The solution contours are smooth and pass continuously through the interfaces. Normal direction profiles for the pressure, velocity and temperature and their derivatives are shown in Fig. 5, at s = 0.78, approximately halfway along the surface of the sphere.

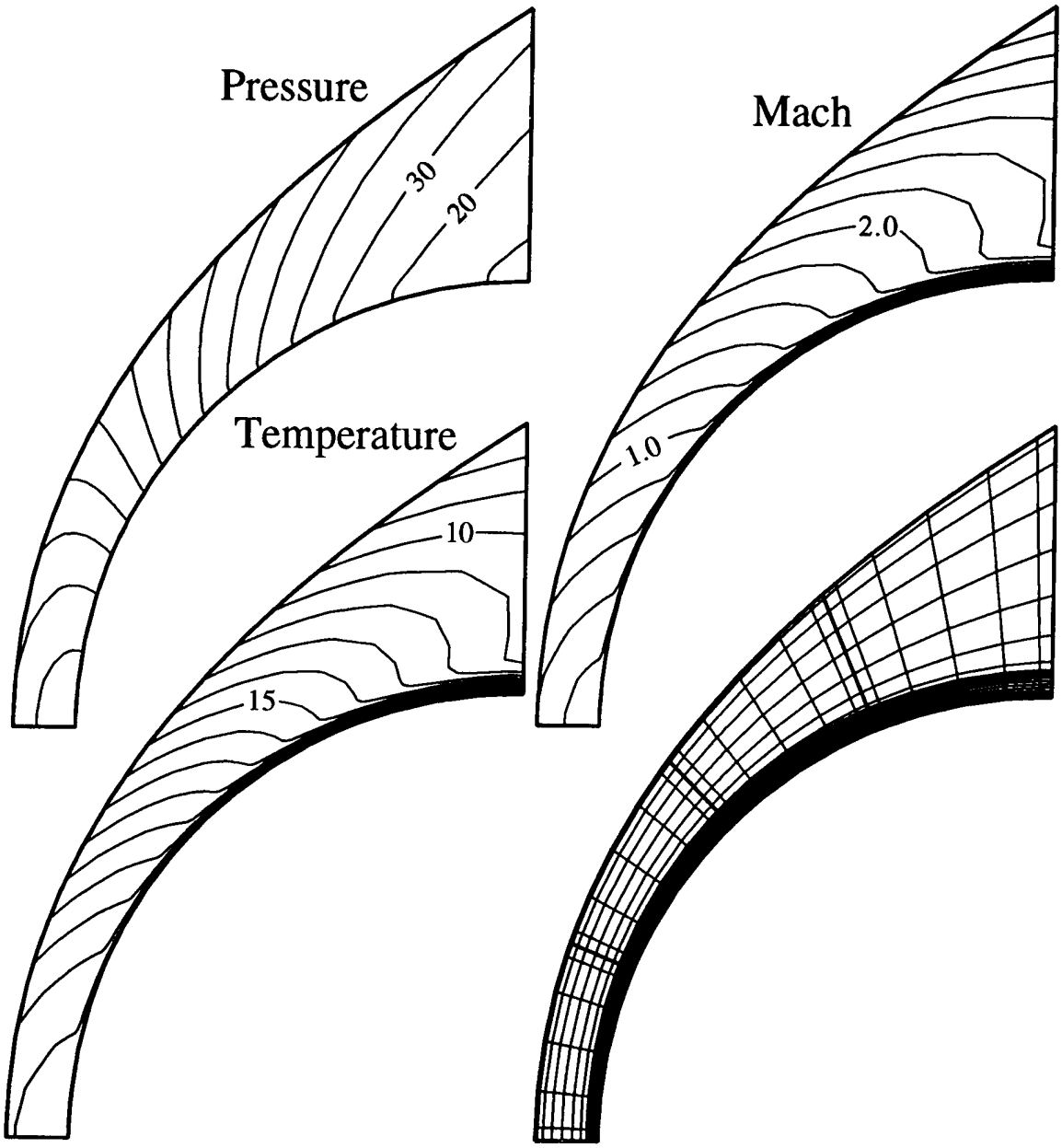

Fig. 3. Solution contours and grid for Case I.

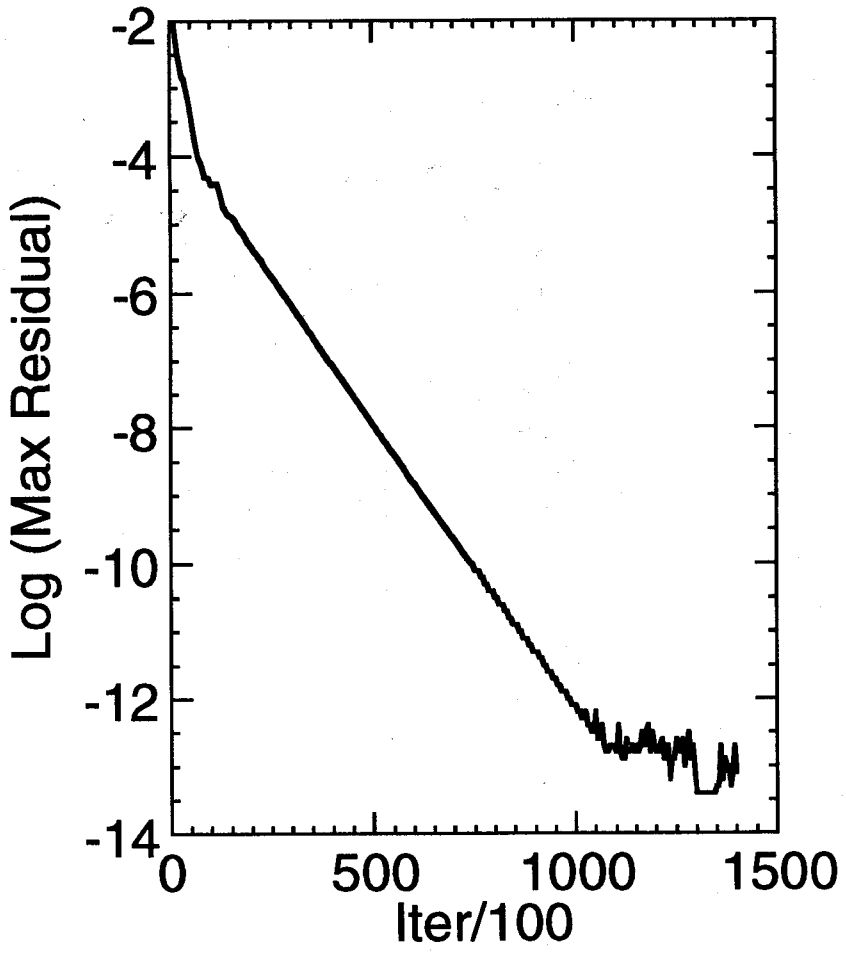

Fig. 4. Convergence of the residual for Case I.

Finally, Fig. 6 plots the pressure coefficient

$$C_p = \frac{p_{body} - p_\infty}{\frac{\gamma}{2} p_\infty M_\infty^2}$$

along the surface of the sphere measured as horizontal distance from the leading edge (See Fig. 1). The result is compared to the inviscid solution computed in Ref. 5, and to the experimental data of Cleary[13]. The viscous computation clearly approximates better the data than the inviscid computation.

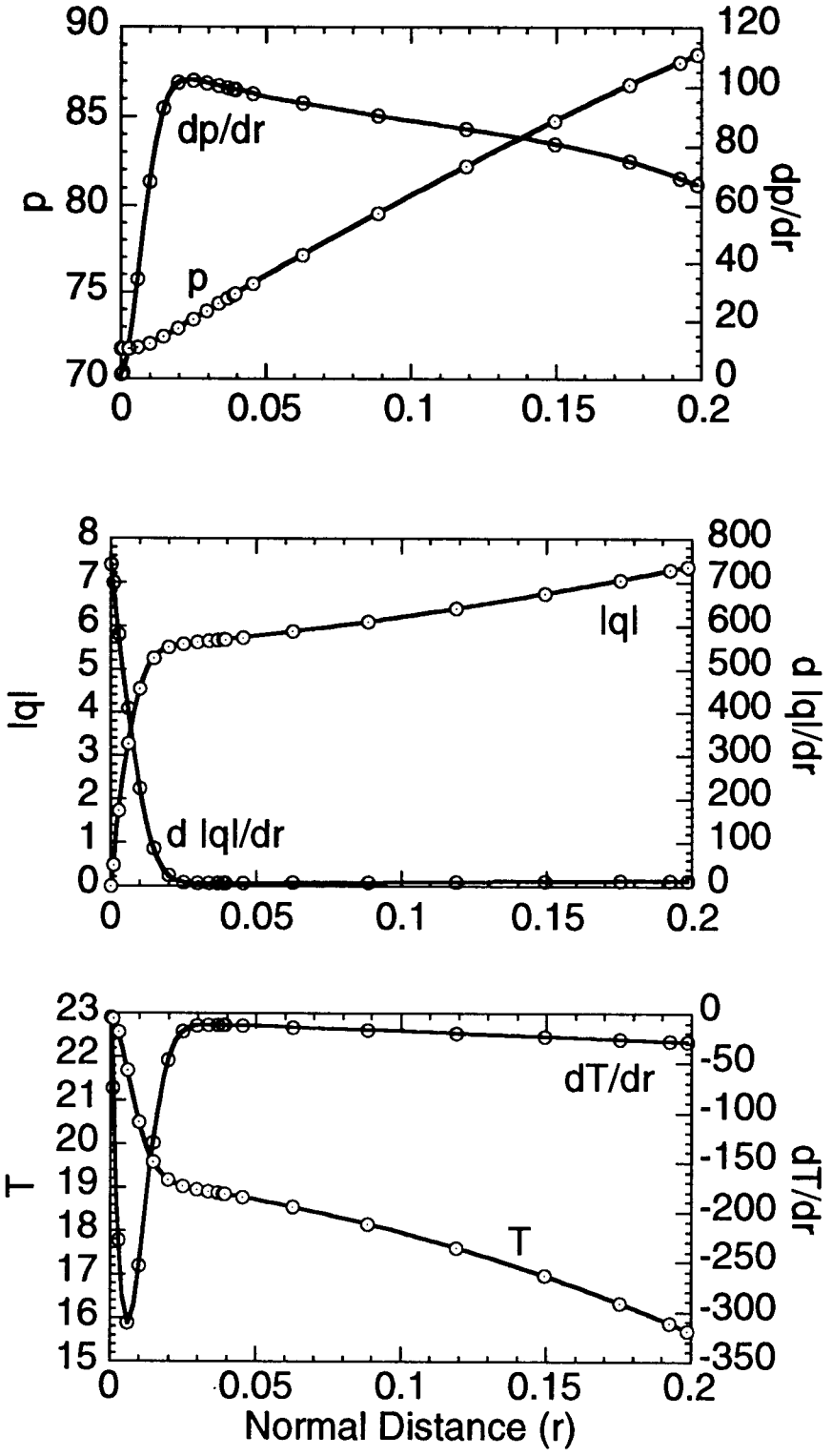

Fig. 5 Solution and derivative profiles at s = 0.78 for Case I.

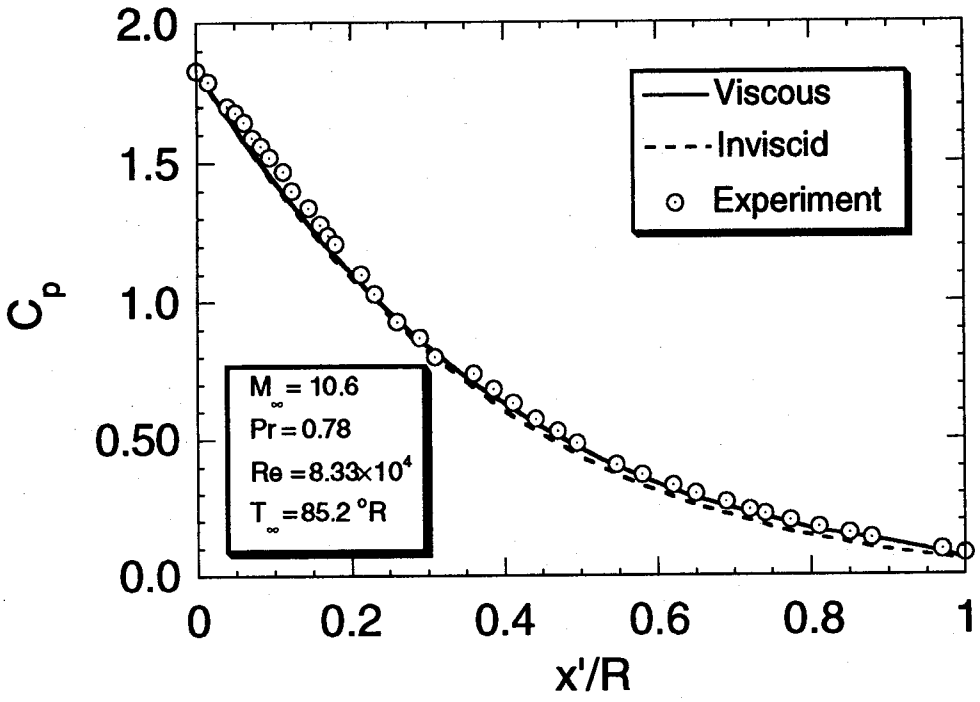

Fig. 6 Pressure coefficient for Case I as a function of horizontal distance from the leading edge.

Case II.

For the second problem, the heat transfer over a cylinder placed in a M = 5.73 free stream was computed, again using eight subdomains. This problem was also solved using a single domain in Ref 9. Fig. 7 shows the contours of the pressure, Mach number and the temperature along with the grid. As before, the solutions are smooth through the interfaces. The heat transfer along the surface of the cylinder is shown in Fig. 8. The results are compared to the experiments of Tiewfik and Geidt[14] and to the finite difference results of Gnoffo[15]. Smoothness of the solution is implied by the continuity of the normal derivative of the temperature across the interfaces.

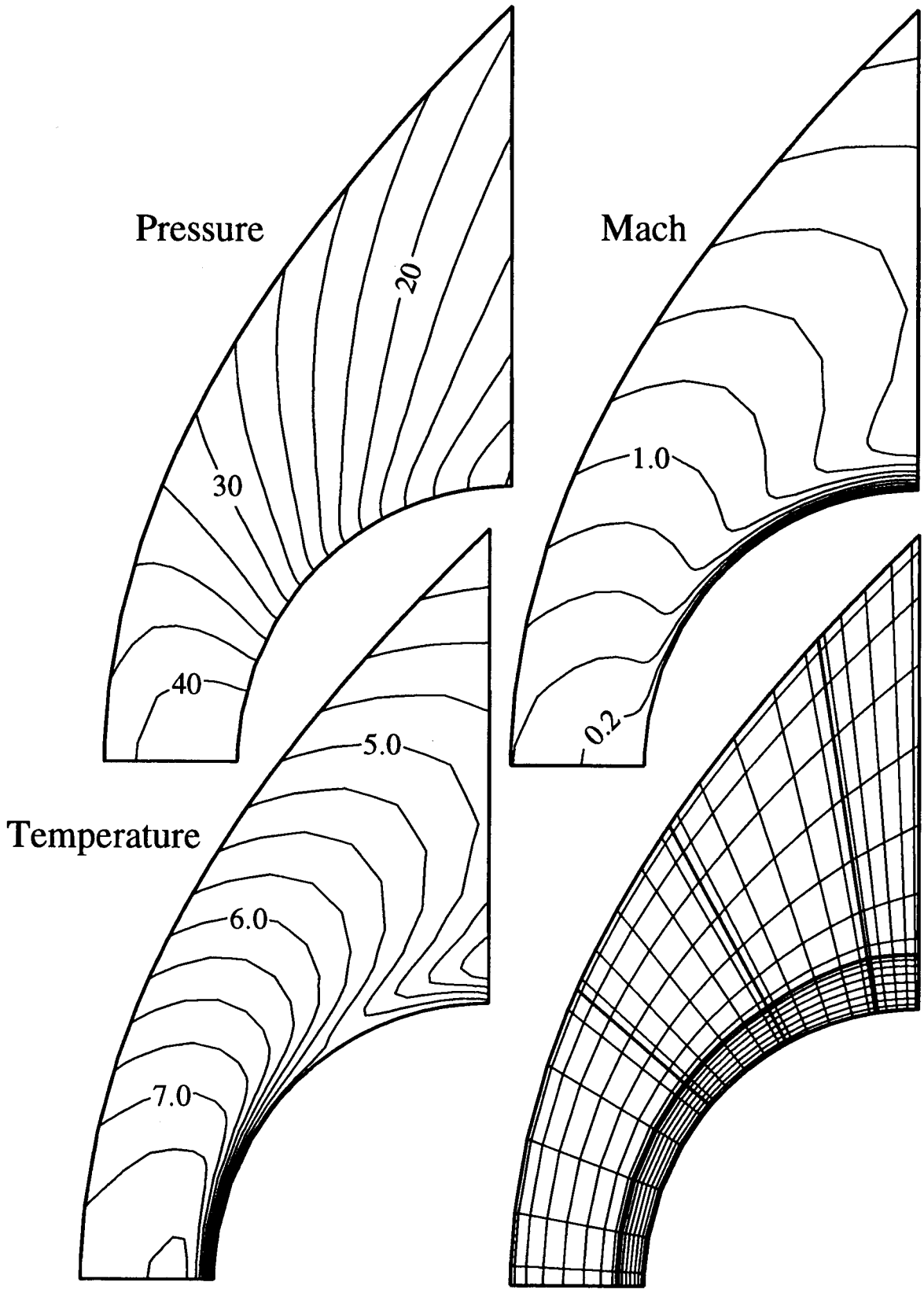

Fig. 7 Solution contours and grid for Case II.

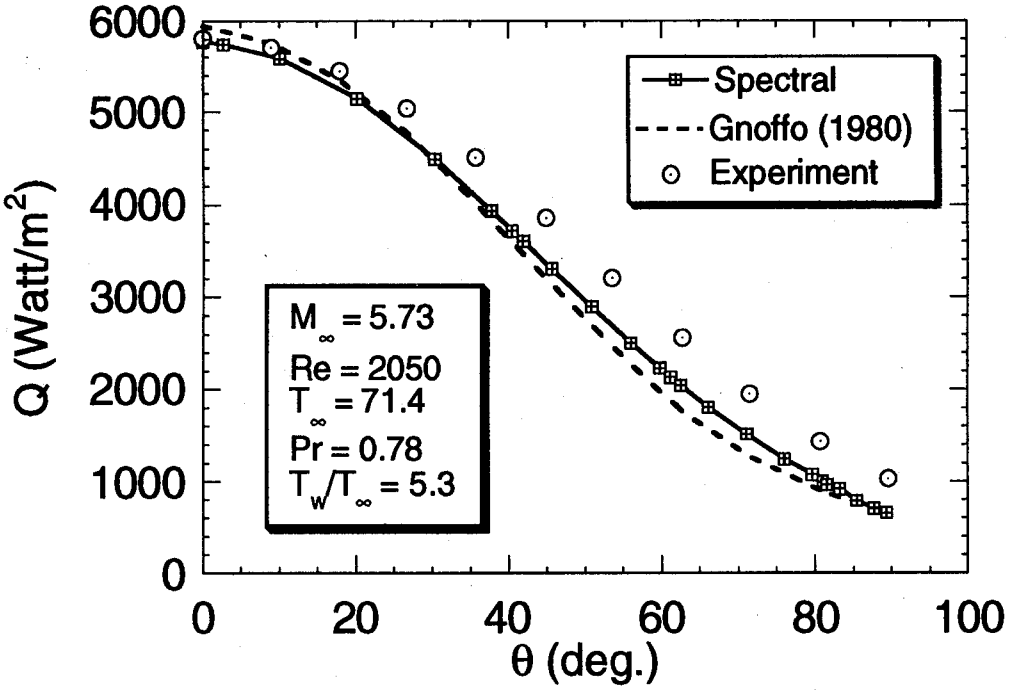

Fig. 8. Heat transfer along the cylinder surface for Case II.

Case III.

A more complex situation is shown in Fig. 9, which depicts the Mach 10.6 flow over a spherically blunted 15^o half-angle cone. The solution contours in Fig. 9 show both the growth of the boundary layer along the cone surface and the shrinking of the entropy layer generated by the shock. The solution was computed on a grid of 14 subdomains. Fig. 10 shows a comparison of the pressure coefficient along the surface of the cone to the inviscid calculation[5] and to the experimental results[13]. Marked by arrows on Fig. 10 are the positions of the subdomain interfaces.

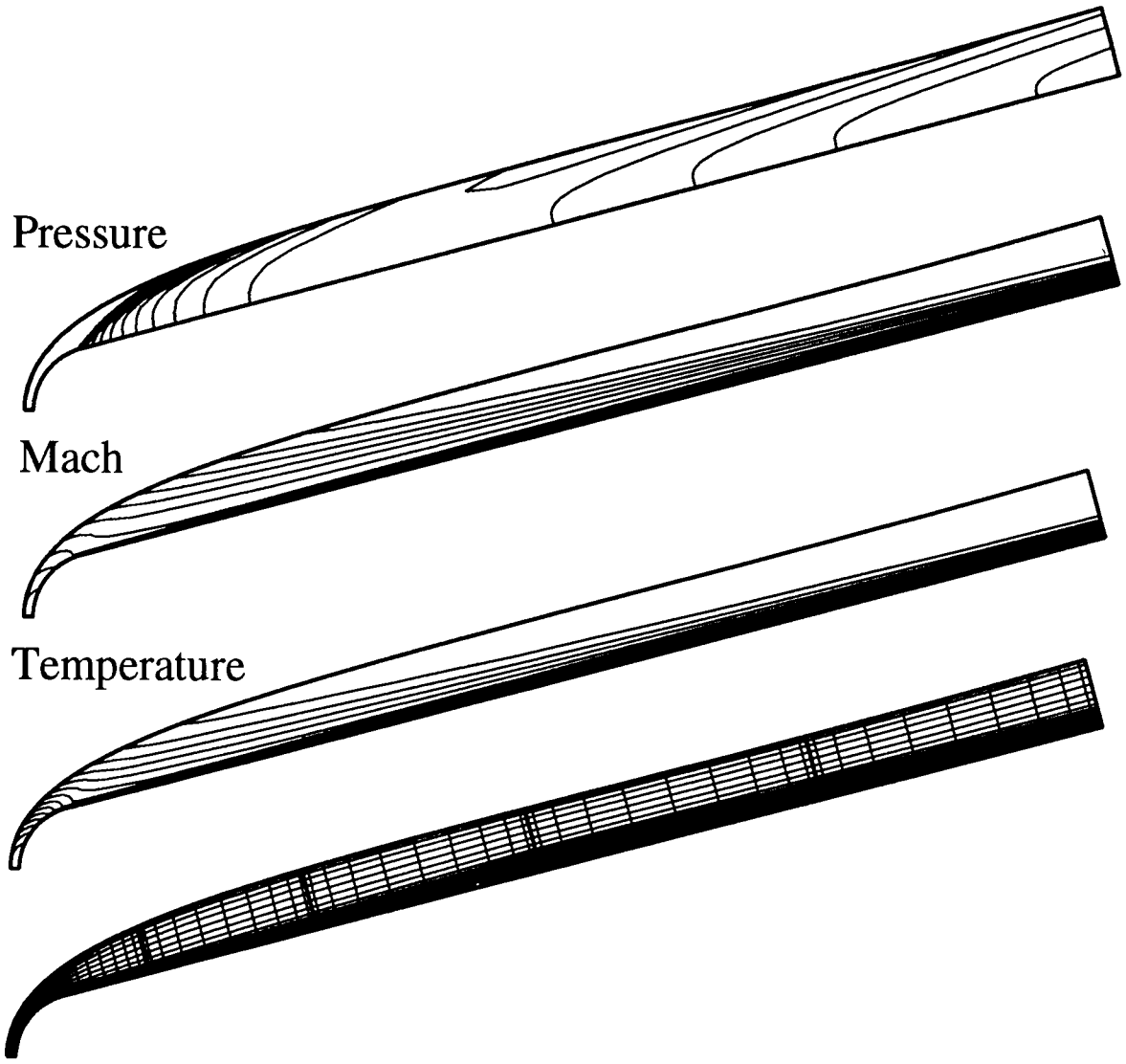

Fig. 9 Solution contours and grid for Case III.

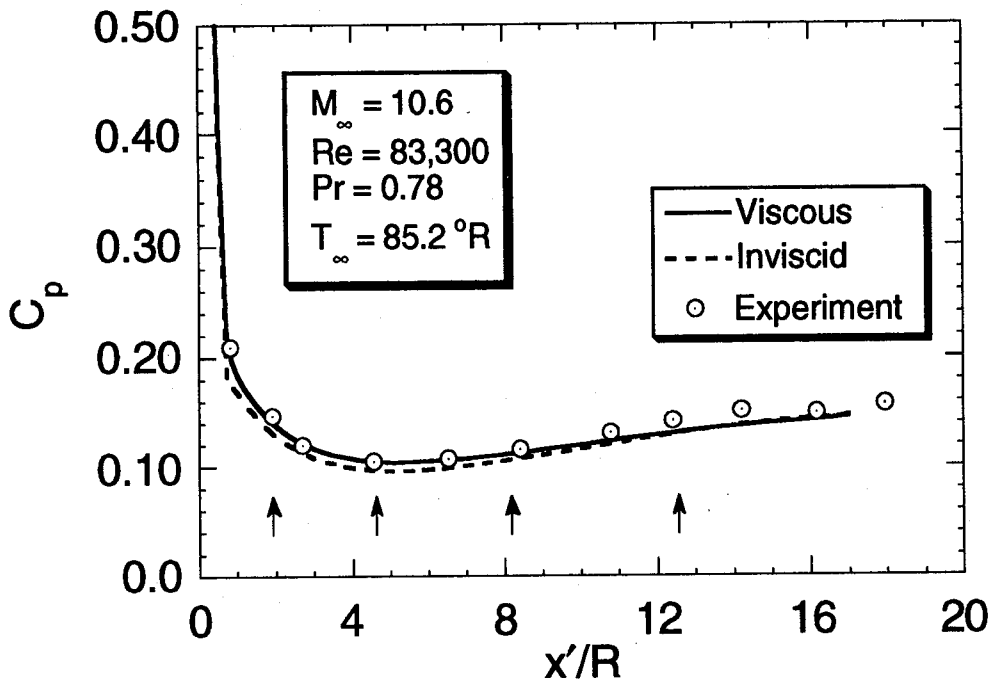

Fig. 10 Pressure coefficient along body surface for Case III.

Case IV.

Case IV is similar to Case III except that the temperature is kept fixed along the surface of the cone. Fig. 11 shows the heat flux normalized to the value of the nose. The computed solution is compared to the experimental results[13].

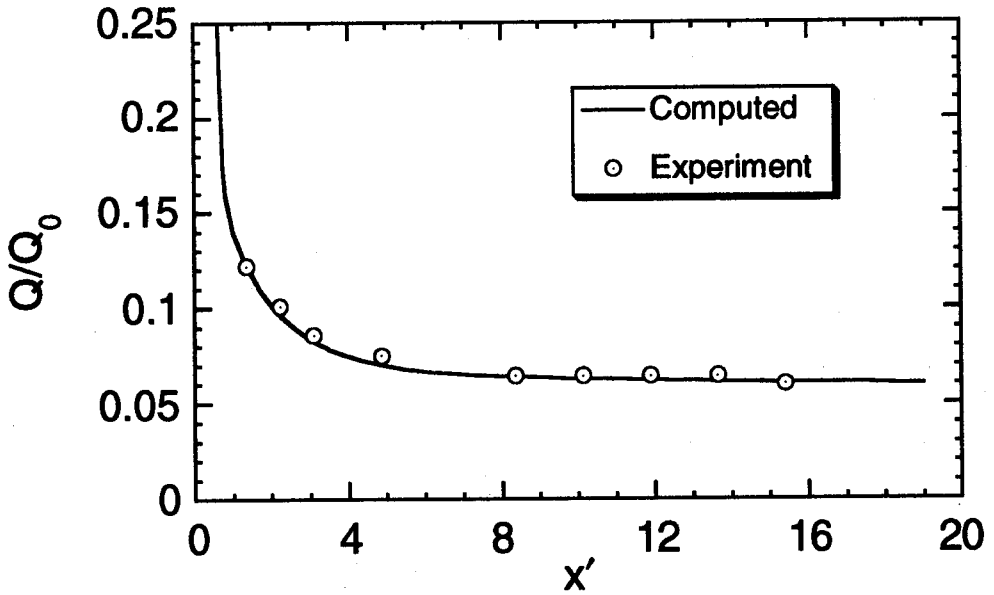

Fig. 11. Heat flux for Case IV.

Case V

As a final example, we make more detailed comparisons of the results of a $M = 25$ flow over a 5^o hyperbolic cone to those of the shock-fitted finite difference code of Ref. 12. The finite difference calculation used 50 points in each direction. Since the ideal gas law, (4), is used, the calculation is meant only for a comparison of the numerical results. This calculation used eight subdomains. Subdomains along the body used 13 points in the normal direction, while those along the shock used seven.

The calculation presented here required 140,000 time steps (starting with the inviscid solution) for the density to reduce the maximum residual in all flow variables 12 orders of magnitude. (See Fig. 12) At 0.285 sec per time step, this means that the calculation required approximately 11 hrs of CPU time on an IBM RS/6000 320H. For comparison purposes, this superscalar machine runs at approximately 4-5 megaflops.

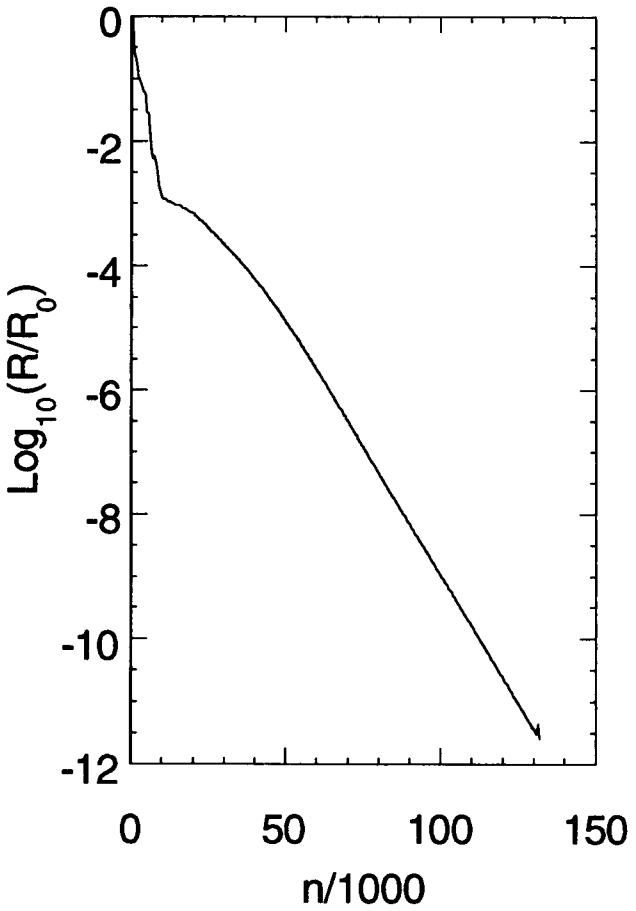

Fig. 12. Convergence of the maximum residual for Case V.

We will first compare the shock position and the wall values of the pressure coefficient, normalized heat transfer and skin friction as a function of the distance along the cone. We will also compare the profiles of the flow quantities in the direction normal to the cone surface at four stations along the length of the cone. We begin by comparing the shock position, as shown in Fig. 13. Plotted is the normal distance of the shock from the body as a function of arc length along the body. Also compared to the multidomain solution is a single domain solution[9] computed on a 20×20 grid so that the number of points in the normal direction is the same.

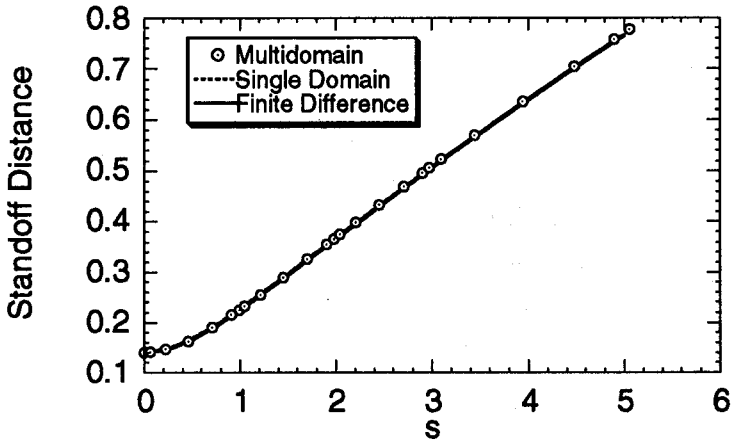

Fig. 13 Shock standoff distance comparing multidomain spectral, single domain spectral and finite difference solutions for Case V.

Fig. 14 compares the pressure coefficient, the heat flux Q, and the skin friction along the body surface as a function of the distance from the nose.

Variations of the pressure, temperature and velocity in the direction normal to the body surface are compared at four stations along the body in Fig. 15. The four stations correspond to the symmetry line and three interfaces that intersect the body. In all cases, we see excellent agreement between the spectral solution and the finite difference solution, and smooth variations through the interfaces.

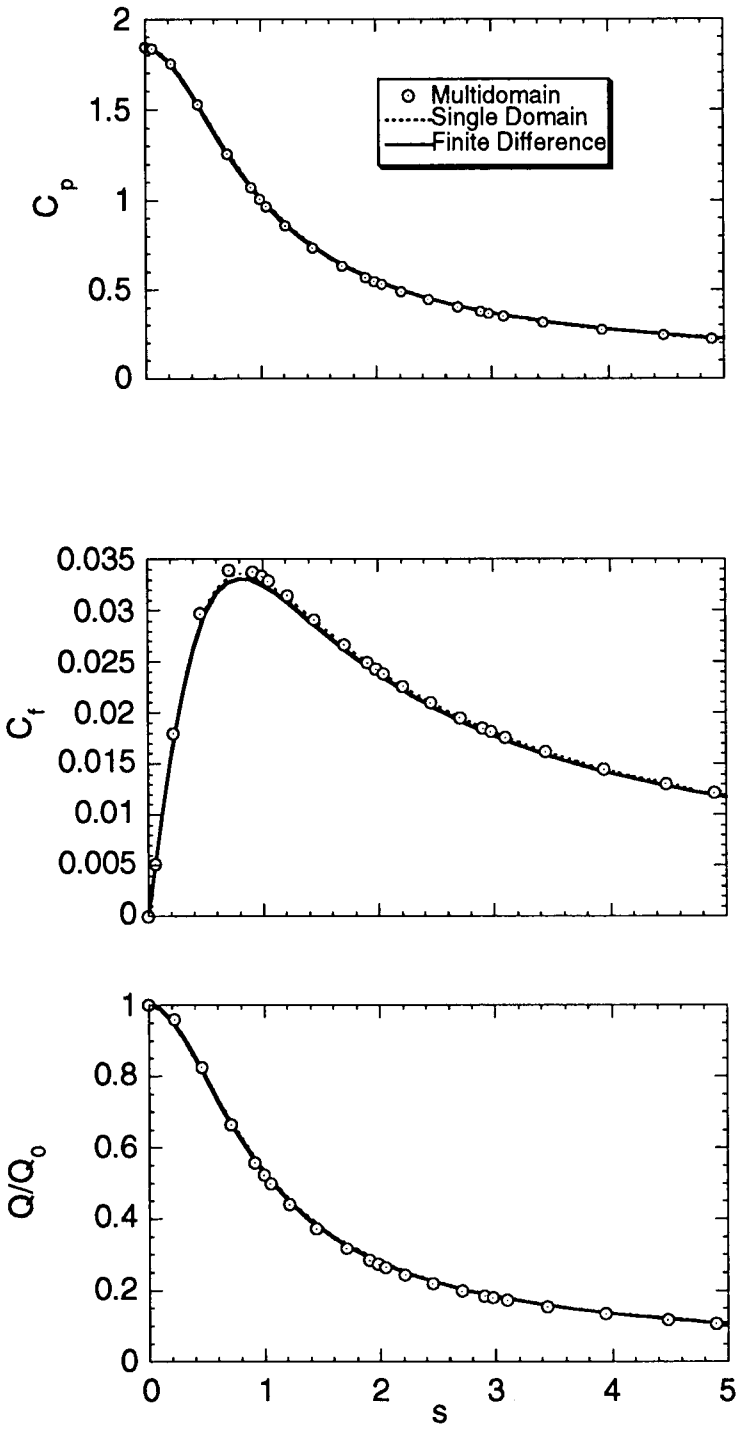

Fig. 14 Body surface quantities for Case V.

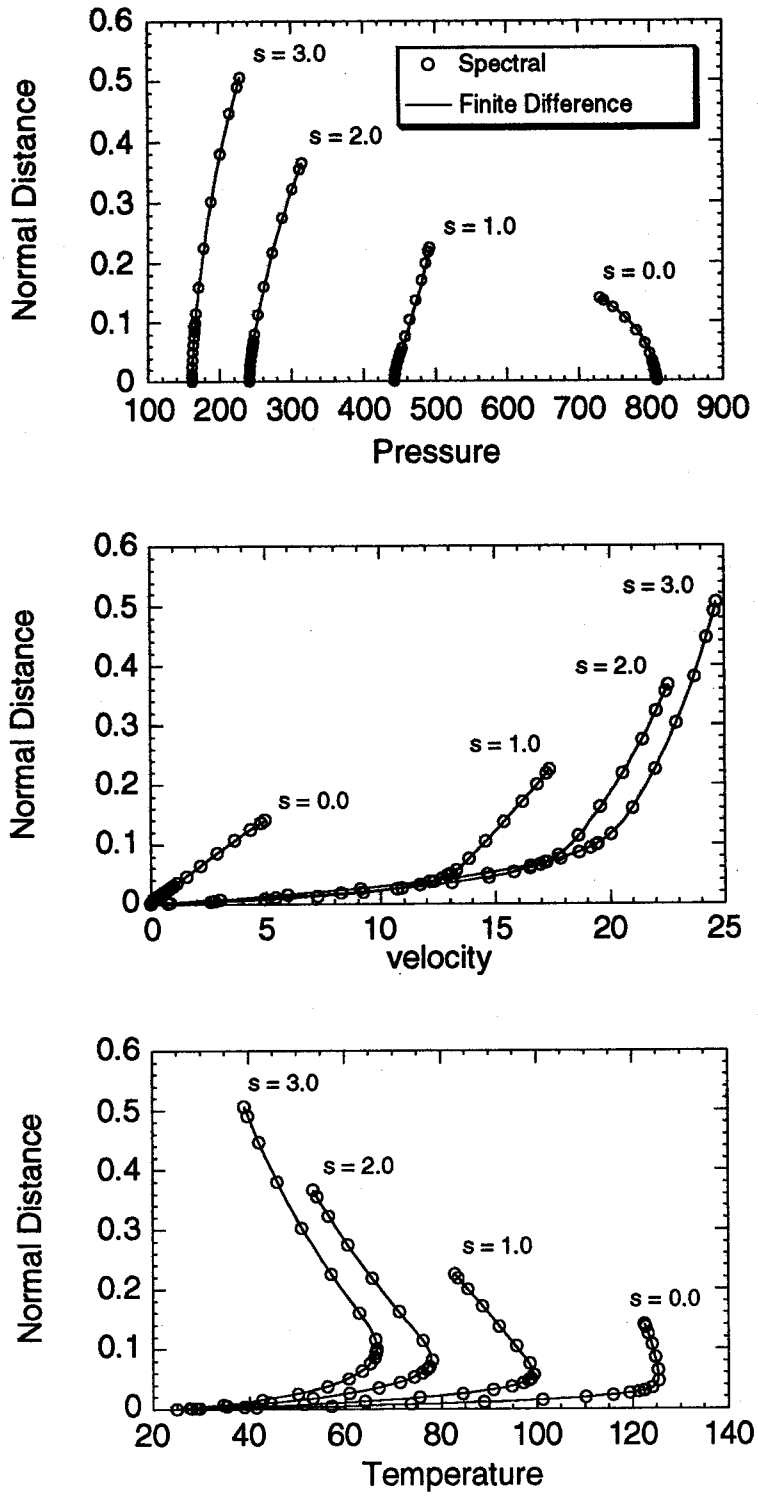

Fig. 15. Normal variation of flow quantities at four stations along the body for Case V.

Conclusions

We have used a multidomain spectral collocation method to solve the compressible Navier-Stokes equations for two-dimensional and axisymmetric supersonic flows over blunt bodies. A main advantage of the method over a single domain method is the ability to distribute easily both subdomain boundary locations and the number of points in each subdomain. Thus, features such as boundary layers can be easily resolved.

At interfaces between subdomains, the advection terms are treated with the characteristic correction method used in Ref. 3 for the inviscid Euler equations. In this way, waves propagate through the interfaces in much the same way as they would for an inviscid flow. The diffusion terms are treated with a penalty method The penalty weakly enforces the continuity of the viscous flux.

The method was applied to five problems. The computations show that the method is stable and that it converged in all cases to a smooth steady-state solution without the need for artificial viscosity or filtering. The results were compared to experimental data, to a finite difference solution, and to a single domain spectral method.

Spectral methods are a high resolution methods and for smooth enough solutions give exponential order accuracy. Phase and dissipation errors are exponentially small. Along with the high accuracy, however, is the fact that the pointwise work is significantly higher than that required by low order finite difference methods. This means that the computations are relatively expensive. Hanley[6] has presented evidence for one space dimension that if high enough accuracy is required, a spectral method can be as much as a factor of seven more efficient than a second order MacCormack scheme. Nevertheless, there is still a serious need for research on methods to accelerate the convergence rate of spectral methods. At this time, we consider the method described here to be appropriate for nose solutions. For longer bodies, the nose solution could be used as a starting solution for a marching code, since the approximation is defined by its Chebyshev interpolant even between grid points.

References

1. Canuto,C., M.Y. Hussaini, A. Quarteroni and T.A. Zang, Spectral Methods in Fluid Mechanics , Springer-Verlag, New York, 1987.

2. Pruett, C.D and Streett, C.L., "A spectral collocation method for compressible, non-similar boundary layers", *International Journal on Numerical Methods in Fluids*, Vol. 13, No. 6, 1991, pp. 713-737.

3. Kopriva, D.A. "Multidomain Spectral Solution of the Euler Gas-Dynamics Equations" *J. Comp. Phys.* Vol. 96 No. 2. , 1991, pp 428-450.

4. Kopriva, D.A., "Spectral Solution of Inviscid Supersonic Flows Over Wedges and Axisymmetric Cones," *Computers and Fluids* , Vol. 21, No. 2, 1992, pp. 247-266.

5. Kopriva, D.A., "Spectral Solutions of High-Speed Flows Over Blunt Cones" *AIAA Journal*, Vol. 31, No. 12, 1993, pp. 2227-2231

6. Hanley, P., "A strategy for Efficient Simulation of Viscous Compressible Flows using a Multi-domain Pseudo-spectral Method", *J. Comp. Phys.* Vol 108, No. 1, 1993 , pp. 153-158

7. D. Sidilkover and G. E. Karniadakis, "Non-Oscillatory Spectral Element Chebyshev Method for Shock Wave Calculations", *J. Comp. Phys.* Vol. 107, No. 1, 1993, pp. 16-22.

8. Kopriva, D.A., "Multidomain Spectral Solution of Compressible Viscous Flows", *J. Comp. Phys.* In Press.

9. Kopriva, D.A., "Spectral Solution of the Viscous Blunt Body Problem", *AIAA Journal*, Vol 31, No. 7, 1993, pp. 1235-1242.

10. Wang, J-P, Y. Nakamura, and M. Yashuhara,, "Global Coefficient Adjustment Method for Neuman Condition in Explicit Chebyshev Collocation Method and its Application to Compressible Navier-Stokes Equations," J. Comp. Phys. Vol. 107, No. 1, 1993, pp. 160-175.

11. Moretti, G., and Salas, M.D., "The Blunt Body Problem for a Viscous Rarefied Gas Flow," AIAA Paper 69-139, Jan. 1969.

12. Kumar, A., and Graves, R.A., "Numerical Solution of the Viscous Hypersonic Flow Past Blunted Cones at Angle of Attack," AIAA paper 77-172, Jan. 1977.

13. Cleary, J.W., "An Experimental and Theoretical Investigation of the Pressure Distribution and Flow Fields of Blunted Cones at Hypersonic Mach Numbers" NASA TN D-2969 ,1965

14. Tewfik, O.K., and Giedt, W.H., "Heat Transfer, Recovery Factor, and Pressure Distributions Around a Circular Cylinder Normal to a Supersonic Rarefied-Air Stream," *Journal of the Aerospace Sciences*, Vol. 27, No. 10,1960, pp. 721-729.

15. Gnoffo, P.A., "Complete Supersonic Flowfields over Blunt Bodies in a Generalized Orthogonal Coordinate system," *AIAA Journal* , Vol. 18, No. 6, 1980, pp. 611-612.

REPORT DOCUMENTATION PAGE

Form Approved
OMB No. 0704-0188

1. AGENCY USE ONLY *(Leave blank)*	2. REPORT DATE	3. REPORT TYPE AND DATES COVERED
	August 1994	Contractor Report

4. TITLE AND SUBTITLE
SPECTRAL SOLUTION OF THE VISCOUS BLUNT BODY PROBLEM. II: MULTIDOMAIN APPROXIMATION

5. FUNDING NUMBERS
C NAS1-19480
WU 505-90-52-01

6. AUTHOR(S)
David A. Kopriva

7. PERFORMING ORGANIZATION NAME(S) AND ADDRESS(ES)
Institute for Computer Applications in Science
and Engineering
Mail Stop 132C, NASA Langley Research Center
Hampton, VA 23681-0001

8. PERFORMING ORGANIZATION REPORT NUMBER
ICASE Report No. 94-73

9. SPONSORING/MONITORING AGENCY NAME(S) AND ADDRESS(ES)
National Aeronautics and Space Administration
Langley Research Center
Hampton, VA 23681-0001

10. SPONSORING/MONITORING AGENCY REPORT NUMBER
NASA CR-194971
ICASE Report No. 94-73

11. SUPPLEMENTARY NOTES
Langley Technical Monitor: Michael F. Card
Final Report
Submitted to AIAA Journal

12a. DISTRIBUTION/AVAILABILITY STATEMENT
Unclassified–Unlimited
Subject Category 64

12b. DISTRIBUTION CODE

13. ABSTRACT *(Maximum 200 words)*
We present steady solutions of high speed viscous flows over blunt bodies using a multidomain Chebyshev spectral collocation method. The region within the shock layer is divided into subdomains so that internal layers can be well-resolved. In the interiors of the subdomains, the solution is approximated by Chebyshev collocation. At interfaces between subdomains, the advective terms are upwinded and the viscous terms are treated by a penalty method. The method is applied to five flows the Mach number range 5-25 and Reynolds number range 2,000 - 83,000, based on nose radius. Results are compared to experimental data and to a finite difference result.

14. SUBJECT TERMS
spectral methods, domain decomposition, viscous flow

15. NUMBER OF PAGES
28

16. PRICE CODE
A03

17. SECURITY CLASSIFICATION OF REPORT	18. SECURITY CLASSIFICATION OF THIS PAGE	19. SECURITY CLASSIFICATION OF ABSTRACT	20. LIMITATION OF ABSTRACT
Unclassified	Unclassified		

NSN 7540-01-280-5500

Standard Form 298(Rev. 2-89)
Prescribed by ANSI Std. Z39-18
298-102

☆U.S. GOVERNMENT PRINTING OFFICE: 1994 - 628-064/23060